RSC Advances

PAPER

View Article Online
View Journal | View Issue

Cite this: *RSC Adv.*, 2021, **11**, 28116

Growth of binary anatase–rutile on phosphorylated graphene through strong P–O–Ti bonding affords a stable visible-light photocatalyst†

Fatima-Ezzahra Zirar,[ab] Aicha Anouar,[a] Nadia Katir,[a] Ihya Ait Ichou[b] and Abdelkrim El Kadib *[a]

Titanium dioxide is an ubiquitous photocatalyst in water-cleaning technologies, being presently the most promising tools to resolve the global issue of sewage treatment. In this framework, titanium dioxide–graphene nanocomposites are discussed as promising visible-light activated photocatalysts but little is hitherto known about the surface and interface chemistry bridging the metal oxide and carbon phases. In an attempt to spotlight this overlooked issue, we herein designed two different hybrid nanocomposites through covalent grafting and growth of titanium dioxide clusters on graphene oxide and on phosphorylated graphene oxide, which affords **GO@TiO$_2$** and **PGO@TiO$_2$**, respectively. While anatase could be selectively harvested on the surface of **GO@TiO$_2$**, biphasic anatase–rutile nucleates could be obtained on **PGO@TiO$_2$**. Thermal annealing treatments improve the metal oxide crystallization and further remove oxygenated groups from the surface of graphene. The interfacial stability of these photocatalysts was also investigated under irradiation, with the graphene support being sensitive to the proximal presence of titanium dioxide. The resulting nanocomposites were also assessed for methylene blue removal through adsorption and photocatalysis. Regardless of their composition, superior photoactivity was noticed for the nanocomposites compared to commercially available degussa that display marginal visible-light photoactivity (11% removal). Within our study, **PGO@TiO$_2$-500** stands as the most active catalyst, allowing nearly quantitative removal of the pollutant from water. The superior performance of **PGO@TiO$_2$-500** can be explained by the highest stability reached through P–O–Ti bonding, its improved crystallinity, and the reduction of the graphene surface during thermal treatment. On a whole, this study provides a blueprint for comparing semiconducting metal oxide grown on tuneable surface-interfacial graphene environments and highlights the utility of surface-engineering graphene sheets to access efficient visible-light oxidation photocatalysts.

Received 8th July 2021
Accepted 6th August 2021

DOI: 10.1039/d1ra05275f

rsc.li/rsc-advances

Introduction

The textile industry consumes about 40 billion tons of water annually to produce the required fabrics, which consequently generate a considerable dyeing effluent that account for nearly 20% of global water pollution.[1] Two procedures are currently applied for discarding dyes waste, namely, adsorption and photo-oxidation.[2,3] An efficient water-cleaning technology should merge the two mechanisms to remove the highest amount of dye waste.[4,5] Additional requirements are the preparation simplicity, its cost effectiveness, and non-toxicity to facilitate the implementation of the whole process at a large scale.[6–11]

Titanium dioxide materials stand definitely as the most efficient photooxidants, with their hegemony being well established compared to their metal oxide counterparts and other related photo-catalysts.[12–14] Their main limitations could be summarized in their low surface area and the lack of photoactivity under visible light.[15,16] To circumvent these setbacks, titanium dioxide has been hybridized with other nanometric phases including metal nanoparticles,[17,18] mesoporous organosilicates,[19–21] quantum dots,[22,23] phosphorus-containing dendrimers,[24–28] and carbon-based nanostructures.[29–32]

In this framework, graphene and its derivatives are on the rise,[33] with graphene-based nanocomposites being expected to revolutionize future nanoscience and nanotechnology.[34,35] The most attractive properties of graphene lie in its high conductivity through faster electron mobility, which is a key enabler in physicochemical processes involving electro- and redox chemistry.[36] Associating titanium dioxide semiconductors and

[a]*Euromed Research Center, Engineering Division, Euro-Med University of Fes (UEMF), Route de Meknes, Rond-point de Bensouda, 30070, Fès, Morocco. E-mail: a.elkadib@ueuromed.org*

[b]*Materials, Photocatalysis and Environment Team, Department of Chemistry, Faculty of Sciences, Ibn Zohr University, B.P. 8106, Dakhla City, Agadir, Morocco*

† Electronic supplementary information (ESI) available: Raman spectra, and recycling experiments of **PGO@TiO$_2$-500**. See DOI: 10.1039/d1ra05275f

graphene sheets in a single nanostructure would therefore led to outstanding visible-light activated photo-catalysts.[37] While precedents in the literature exist for the physical mixing of the carbon and metal oxide phases,[38,39] little is known concerning their covalent grafting from soluble precursors through wet chemistry and their growth during thermal treatment.[40,41] Physical mixing faces several drawbacks including severe leaching and bleaching, which are commonly encountered when the active species are only entrapped within the carrier. Besides, only graphene oxide was used as a selected support while no other functional graphene derivative has been assessed for such a purpose. Although oxygenated functional groups are pivotal for **GO** dispersion in the liquid phase medium, they are labile, thermo- and photo-sensitive, and are prone to faster degradation, including under irradiation.[42,43] These facts associated to the scarcity of the literature in related materials hinder comparative studies to glean a deeper understanding on the interfacial properties of the resulting nanocomposites, which is mandatory for the rational design of stable and durable active photo-catalysts. Initial investigations in this framework focused on comparing the performance of graphene and its forebears, carbon nanotubes and fullerene.[44] Considering the unlimited possibilities of graphene-surface functionalization, later research recalled rather the interest of the interfacial engineering of graphene sheets to maximum its performance.[45] Keeping in mind the excellent stability of P–O–Ti bridges,[24–27] we envisioned that such an approach could improve the interfacial stability of titanium dioxide grafted on graphene support.

We have recently succeeded in functionalizing graphene oxide with a set of phosphorus derivatives,[46,47] and unambiguously established an improvement in their thermal stability.[46] With these materials in hand, we embarked herein to assess the growth of titanium dioxide on two different graphene surfaces (**GO** *versus* **PGO**) and to elucidate their behavior during irradiation and for the photo-oxidation of methylene blue as a representative textile dye pollutant.

Results and discussion

Synthesis of the materials

Graphene oxide (**GO**) was prepared by graphite oxidation using Hummers' method, followed by ultrasonication.[48] **GO** oxide displays various oxygen functional groups on its surface (alcohols, epoxides, carboxylic acids, carbonyls), which impart it with an excellent colloidal stability in a wide range of solvents.[49] These oxygen functional groups usually serve as anchoring sites to immobilize metal nanoparticles but are prone to decomposition under high temperature treatment.[50,51] To overcome this issue, we have previously succeeded in improving the thermo-oxidative stability of graphene through surface phosphorylation using $POCl_3$.[46] The resulting phosphorylated graphene oxide (**PGO**) displayed an impressive increase in the half-weight decomposition temperature from $T_{50} = 391$ °C for **GO** to $T_{50} = 758$ °C for **PGO**.[46] We have indeed decided to use both **GO** and **PGO** as the support to grow titanium dioxide clusters (Fig. 1).

The **GO@TiO$_2$** and **PGO@TiO$_2$** materials were synthesized *via* a one-pot sol–gel method, starting from titanium tetraisopropoxide as the titanium dioxide source and **GO** or **PGO** as the support. The presence of several functional groups on the surface of **GO** or **PGO** allows for the anchoring and growth of metal oxide nuclei. Following the anchoring of metal-oxo-species on the **GO** or **PGO** support, further hydrolysis and condensation during the heating step induce the growth of the metal oxide on the surface. After extensive washing to remove non-covalently grafted species, the harvested solid materials (**GO@TiO$_2$** and **PGO@TiO$_2$**) were dried and subjected to textural and structural analyses (Fig. 2).

In XRD, well-resolved peaks assignable to the crystalline anatase phase are observed at 25.5°, 37.9°, 47.6°, 54.5°, 62.7°, 69.1°, and 75.3° corresponding to the (101), (004), (200), (105), (213), (116), and (215) planes, respectively, for **GO@TiO$_2$** while a mixture of anatase and rutile seems to be formed for **PGO@TiO$_2$** by the appearance of similar peaks observed for

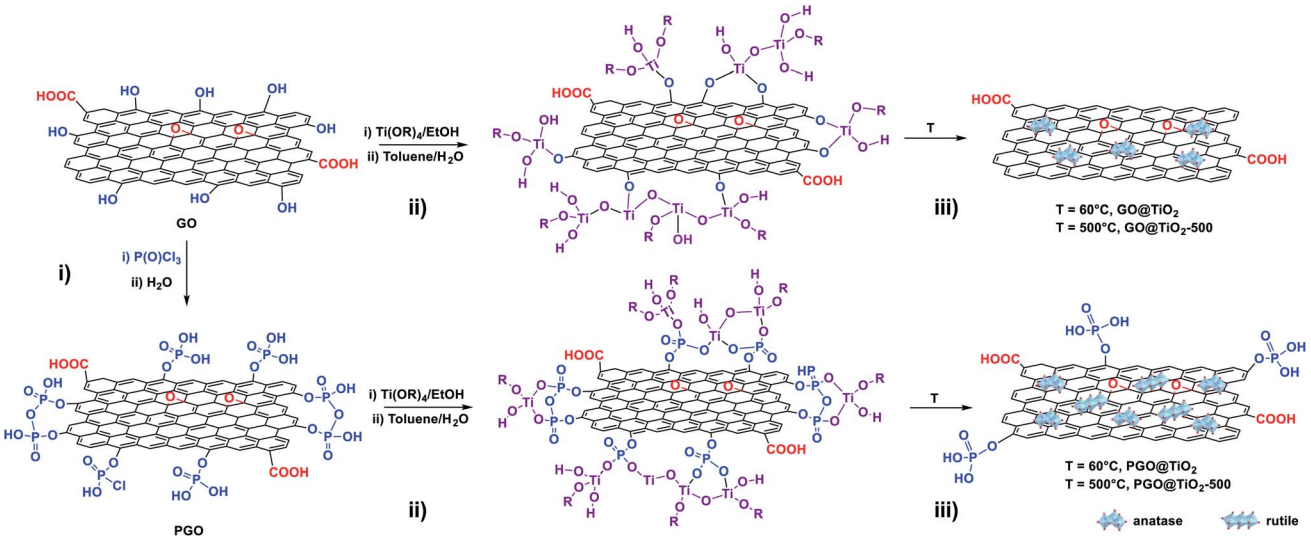

Fig. 1 Schematic illustration of the synthetic approaches for the (i) phosphorylation of GO (**PGO**), (ii) one-pot sol–gel synthesis, and (iii) heating at 60 °C (**GO@TiO$_2$** or **PGO@TiO$_2$**), followed by thermal annealing at 500 °C (**GO@TiO$_2$-500** or **PGO@TiO$_2$-500**).

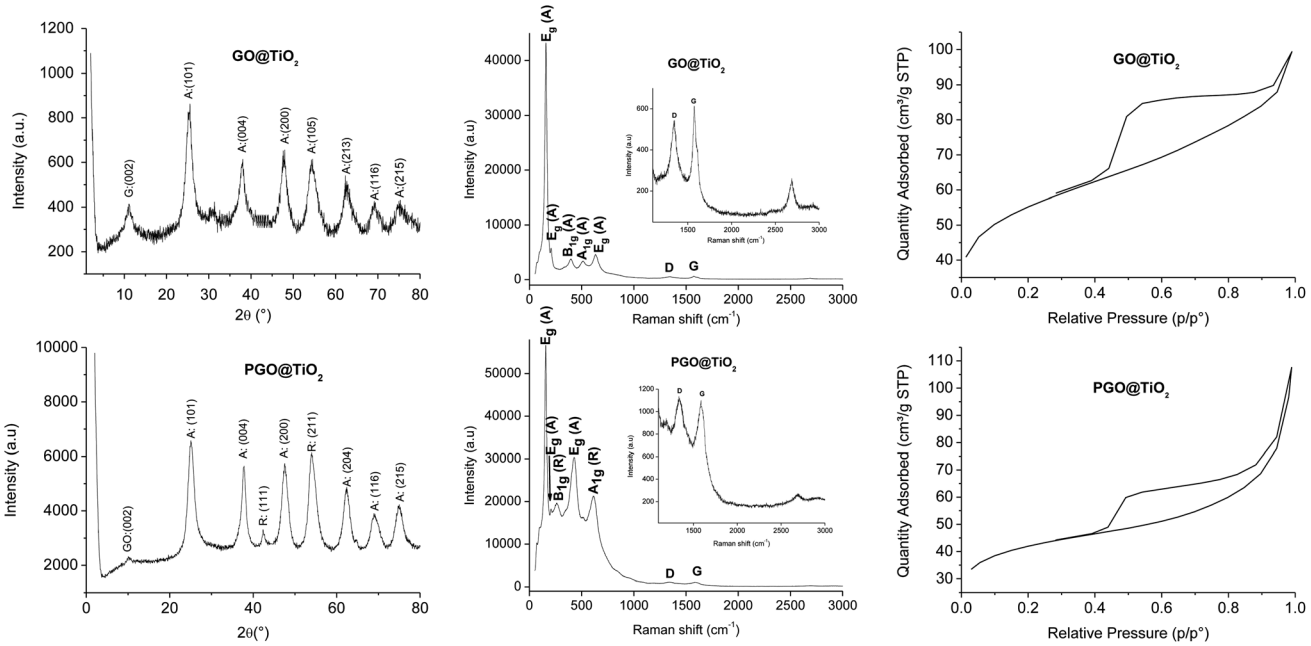

Fig. 2 X-ray diffractogram (left), Raman spectra (center), and N_2 adsorption–desorption isotherms (right) of **GO@TiO$_2$** (top) and **PGO@TiO$_2$** (bottom).

GO@TiO$_2$ corresponding to the anatase phase and new peaks at 42.3° and 54° corresponding to the (111) and (211) planes of the rutile phase of TiO_2 (JCPDS card no. 21-1272 for anatase and JCPDS card no. 21-1276 for rutile TiO_2) (Fig. 2, left). The discrepancy observed between **GO** and **PGO** in nucleating different species provides a clear evidence of the role of surface chemistry in promoting the well-defined metal oxide phase. Notably, the peak corresponding to the (002) plane of **GO** at 11.2° can be barely distinguished in **PGO@TiO$_2$** while its intensity in **GO@TiO$_2$** is more significant. This suggests that the amount of Ti loaded on **PGO** is more important compared to that supported using **GO**. Raman spectroscopy further corroborates these results as the anatase and rutile phase could be easily discriminated.[52] The different modes observed in the Raman spectrum of **GO@TiO$_2$** at 157, 206, 396, 510, and 632 cm^{-1} correspond to E_g, E_g, B_{1g}, A_{1g}, and E_g of the anatase phase, respectively. In the case of **PGO-TiO$_2$**, the different modes displayed in the Raman spectrum at 155, 206, 260, 428, 512, and 613 cm^{-1} correspond to E_g (anatase), E_g (anatase), B_{1g} (rutile), E_g (rutile), A_{1g} (anatase), and A_{1g} (rutile) (Fig. 2, center).

Besides, both the nano-hybrids display additional bands at 1347 and 1573 cm^{-1} for **GO@TiO$_2$** and at 1341 and 1586 cm^{-1} for **PGO@TiO$_2$**. The I_D/I_G ratio found for **GO@TiO$_2$** is 0.89, which is much lower than 1.02 recorded for **PGO@TiO$_2$**. The I_D/I_G ratios found for **GO** and **PGO** are 0.925 and 1.25, respectively. The increased ratio found for PGO-based materials could be associated with the incorporation of phosphate moieties into the surface of graphene support.

The interplay of titanium oxide species with the graphene surface has been previously elucidated through XPS analyses.[24] The apparition of the typical Ti (2p) binding energy of tetrahedral Ti^{4+} at 459.0 eV for both **GO@TiO$_2$** and **PGO@TiO$_2$** indicates the presence of titanium on the surface of the graphene support. Interestingly, the signal of phosphorus is still present at 134.0 eV for **PGO@TiO$_2$**, indicating that grafting did not remove the phosphorus species. The presence of several components in the O (1s) region (binding energy at 530.4 eV and 531.8 eV) unambiguously confirm the presence of covalent bonding (both C–O–P and P–O–Ti) in the graphene surface.[24]

Interestingly, **PGO** was found to be more reactive toward titanium alkoxide compared to conventional **GO**, as confirmed from ICP analyses (2.3 wt% Ti in **GO@TiO$_2$** *versus* 5.17 wt% Ti in **PGO@TiO$_2$**). This discrepancy can be associated with the presence of different kinds of functional groups on **PGO** support, *i.e.*, (i) additional phosphate moieties are grafted on the surface of **PGO**, allowing for the anchorage of an appreciable amount of titanium alkoxide, and (ii) the high stability of P–O–Ti bridges formed at the material interface (compared to C–O–Ti), thereby precluding the leaching of titanium-oxo-alkoxo species back to the solution. The common use of organophosphonic and organophosphonate coupling reagents to coat the external surface of metal oxides through stable P–O–M bonding (M = Ti, Al, Zr, Sn, V) consolidate these assumptions.[53–58]

Nitrogen adsorption–desorption shows an interesting open mesoporous framework of the two materials (Fig. 2, right). An appreciable surface area of 186 $m^2\ g^{-1}$ was observed for **GO@TiO$_2$**, while a smaller surface area of 135 $m^2\ g^{-1}$ was found for **PGO@TiO$_2$**. The decrease in the surface area for **PGO@TiO$_2$** can be accounted for by the loaded amount of Ti on both the materials or by the functionalization of **GO** with phosphate groups, which might block some pores.[59] However, the recorded value remains much higher for titanium dioxide-based materials, where the most popular Degussa P25 displays a marginal surface area of 48 $m^2\ g^{-1}$.

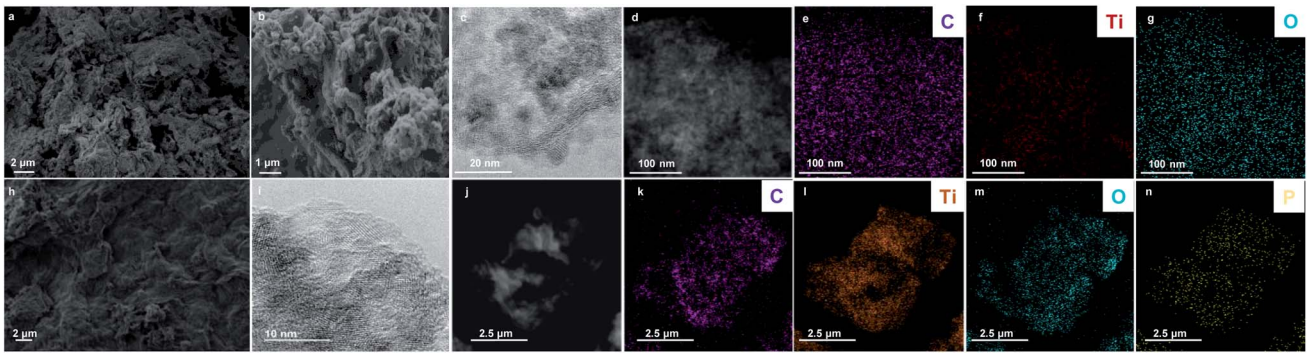

Fig. 3 FESEM images of **GO@TiO$_2$** (a and b) and **PGO@TiO$_2$** (h), HRTEM images of **GO@TiO$_2$** (c) and **PGO@TiO$_2$** (i), STEM images of **GO@TiO$_2$** (d) and **PGO@TiO$_2$** (j), and associated EDX mapping of **C** (e), **Ti** (f), **O** (g) elements for **GO@TiO$_2$** and of **C** (k), **Ti** (l), **O** (m), and **P** (n) elements for **PGO@TiO$_2$**.

The morphology of **GO@TiO$_2$** and **PGO@TiO$_2$** was investigated using FESEM analysis (Fig. 3a, b and h). The two materials are quite similar but different from their parents **GO** or **PGO** with the altered texture, being a direct consequence of the formation of titanium dioxide on the graphene surface. HRTEM was further used to get insight at the nanoscale level (Fig. 3c and i). The crystallinity of the supported metal oxide can be observed in both the cases although to a less extent in the case of **GO@TiO$_2$**. The crystallinity is more pronounced in the case of **PGO@TiO$_2$**, probably due to the amount of Ti loaded on the different supports. Elemental mapping using EDX clearly shows the presence of C, O, and Ti for **GO@TiO$_2$** and the homogeneous distribution of C, O, Ti, and P elements for **PGO@TiO$_2$** (Fig. 3e–g and k–n).

Next, these hybrid materials were subjected to thermal annealing treatment at $T = 500$ °C under nitrogen atmosphere and the resulting materials were denoted as **GO@TiO$_2$-500** and **PGO@TiO$_2$-500**.

The Raman spectrum of **GO@TiO$_2$-500** displays several peaks at 146, 198, 400, 515, and 635 cm^{-1} corresponding to the E_g, E_g, B_{1g}, A_{1g}, and E_g modes of the anatase phase, respectively. Besides, new peaks are observed at 438 and 615 cm^{-1}, assignable to the rutile phase. For **PGO@TiO$_2$-500**, peaks at 147, 206, 260, 414, and 612 cm^{-1} correspond to the E_g (anatase), E_g (anatase), B_{1g} (rutile) E_g (rutile), and A_{1g} (rutile) modes, respectively (Fig. 4). These observations indicate that thermal annealing affects the crystalline structure of **GO@TiO$_2$-500** through the appearance of a new crystalline rutile phase. In contrast, no noticeable variation could be detected for **PGO@TiO$_2$-500**, for which the presence of phosphorus precludes thermally-induced phase transformation, thereby keeping the same crystalline structure as was previously observed for phosphorus-containing materials.[19–21] **GO@TiO$_2$-500** and **PGO@TiO$_2$-500** display additional Raman shifts corresponding to the D and G bands at 1355 and 1598 cm^{-1} for the former and at 1348 and 1587 cm^{-1} for the latter, respectively. The blue shift of the D and G band observed in **PGO@TiO$_2$-500** has been previously attributed to the incorporation of phosphate functional groups into the structure of graphene oxide. The I_D/I_G ratio found for **GO@TiO$_2$-500** is 0.875, while that found for **PGO@TiO$_2$-500** is 0.897. These ratios are smaller than those of the native materials (0.89 for **GO@TiO$_2$** and 1.02 for **PGO@TiO$_2$**), pointing to the occurrence of chemical reduction on the surface of **GO** and **PGO** during thermal treatment under nitrogen atmosphere.[60]

The morphology of the thermally-annealed nanocomposites was assessed by FESEM and in both cases, small TiO_2 are distributed on the surface of the carbon nanosheets (Fig. 5). Clustered metal oxide supported on **PGO** appears to be smaller, evidencing the role of phosphorus on controlling the growth of TiO_2 particles.[25] EDX elemental mappings reveal the presence and homogenous distribution of Ti and O as the main elements on **GO@TiO$_2$-500** and Ti, O, and P for **PGO@TiO$_2$-500**.

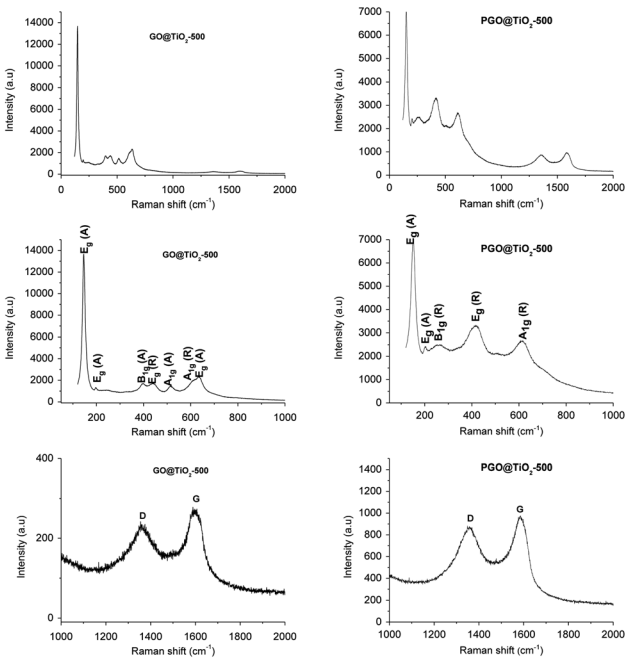

Fig. 4 Raman spectra of **GO@TiO$_2$-500** and **PGO@TiO$_2$-500** (top) and Raman spectra of **GO@TiO$_2$-500** and **PGO@TiO$_2$-500** in the 0–1000 cm^{-1} Raman shifts range (middle) and in the 1000–2000 cm^{-1} Raman shifts range (bottom).

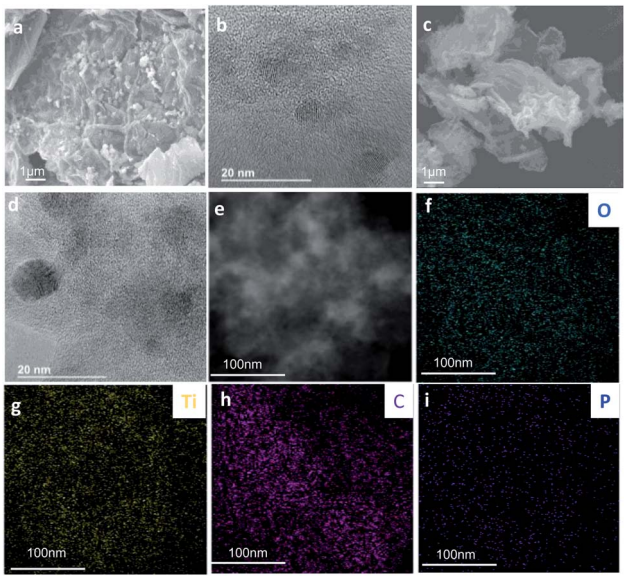

Fig. 5 FESEM image (a) and HRTEM image (b) of **GO@TiO$_2$-500**, FESEM image (c), HRTEM image (d), and STEM image (e) of **PGO@TiO$_2$-500** and associated EDX elemental mappings of **O** (f), **Ti** (g), **C** (h), and **P** (i) elements.

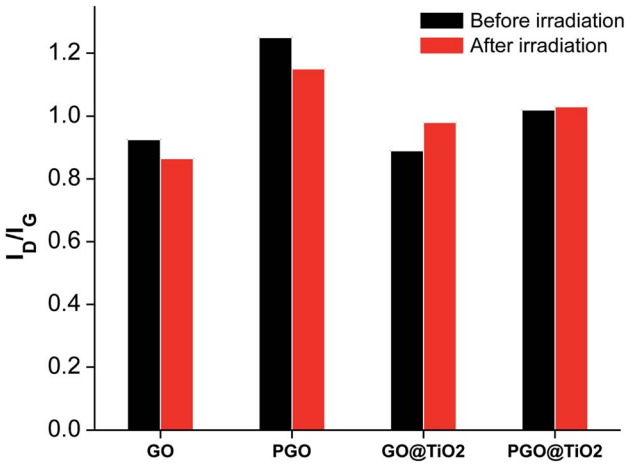

Fig. 6 Variations in the I_D/I_G ratios determined from the Raman spectra of **GO**, **PGO**, **GO@TiO$_2$**, and **PGO@TiO$_2$** before and after irradiation.

Stability of graphene-based materials toward light irradiation

Since TiO_2–graphene nanocomposites are massively used for the photocatalytic degradation of pollutants, the study of their photo-stability is of paramount importance. In fact, the disintegration of graphene oxide or reduced graphene oxide into smaller poly-aromatic hydrocarbon fragments would raise more environmental concerns, which could overshadow their photocatalytic benefits.[43] The chemical and physical tailoring of graphene was accomplished using a TiO_2 photomask where highly active oxygen species formed upon irradiation of the photomask act as chemical scissors.[61] TiO_2 was also used as a mediator for the chemical reduction of graphene oxide.[62] However, all these observations rely on the metal oxide and carbon phase physically dispersed and none of them have investigated nanocomposites designed through the covalent grafting of the two antagonist phases.

To get further insight, we relied on Raman spectroscopy to assess the interfacial stability of **GO@TiO$_2$** and **PGO@TiO$_2$** toward light irradiation. An increase in the I_D/I_G ratio in the Raman spectrum was regarded as an indicator of the structural change upon photocatalytic oxidation.[63] We first assessed the stability of **GO** and **PGO** under visible-light irradiation (Fig. S1 and S2†). As it can be seen in Fig. 6, for both **GO** and **PGO**, the I_D/I_G found after irradiation is 0.864 and 1.15, respectively (against 0.925 and 1.25 for non-irradiated **GO** and **PGO**, respectively). The decrease in the ratio implies a reduction in both the materials with a restoration of the sp^2 domains. This trend was previously observed and attributed to the decomposition of the oxidized areas in the **GO** flakes. Moreover, the excitation of the aromatic domains in **GO** leads to charge separation and the electrons partake in the reduction of **GO**.[64] For **GO@TiO$_2$**, after irradiation, the I_D/I_G ratio increases from 0.89 to 0.98 (Fig. 6 and S3†). This increase in the I_D/I_G ratio along with the hypsochromic shift of the D and G bands suggests the enhancement of the structural defects due to light irradiation. Besides, new peaks assignable to the rutile phase could be observed, in a similar way to the variation noticed for **GO@TiO$_2$-500** after thermal treatment. In a previous study, it was found that irradiation with visible light of the anatase nanoparticles under oxygen-poor conditions is an athermal process that leads to phase transition from the anatase to the rutile phase.[65]

In contrast, the irradiation of **PGO@TiO$_2$** did not significantly change the I_D/I_G ratio, suggesting the highest stability of the phosphorylated carbon surface and/or the absence of oxygenated defects compared to those existing in **GO** (Fig. S3†). This brings additional evidence for the highest interfacial stability of this material owing to the presence of P–O–Ti bridges. Indeed, depending on their surface state, irradiation can have an effect on the structure of graphene and on the crystalline phase of titanium dioxide. In **PGO@TiO$_2$**, we have previously found that bulk amorphous phases coexist along with the crystalline biphasic TiO_2 formed through our one-pot procedure.[46] After irradiation, these amorphous regions crystallize into the anatase phase. The presence of phosphorus species (phosphate groups) is well established to hinder the thermodynamically favorable transition from anatase to rutile.[25,66] For **GO@TiO$_2$**, irradiation induces phase transition from anatase to rutile, which is set to occur upon light irradiation.[65] Indeed, attention should be paid to the stability of the corresponding photo-catalysts under applied experimental conditions, concomitantly with a deeper characterization before and after irradiation.

Photocatalytic studies

While the benefits of adding graphene to titanium dioxide are already reported, it is not clear whether surface phosphorylation is good or detrimental for their photo-activity. We therefore

embarked to assess the photocatalytic performance of all graphene-based photo-catalysts for methylene blue degradation from waste water. We also benchmarked different graphene-based materials as well as the most popular and commercially available Degussa P25 titanium dioxide.

All nanocomposites based on graphene–titanium dioxide displayed significant photo-oxidation activity, being superior to the commercial Degussa P25 that is known to be active only under UV irradiation. This ultimately points to the improvement reached by adding photosensitizing graphene to the material substructure. We have also noticed that **PGO@TiO$_2$** was much more reactive compared to **GO@TiO$_2$**, a fact that could be attributed to the presence of biphasic anatase–rutile and their improved stability through P–O–Ti bonding compared to its conventional analogues attached through C–O–Ti bridges. Besides, thermally treated materials **GO@TiO$_2$-500** and **PGO@TiO$_2$-500** are more reactive compared to their parent precursors, with the same trend being observed (Fig. 7). In quantitative numbers, 73% methylene blue removal was recorded for **GO@TiO$_2$** after 60 min treatment, while 93% was reached with **PGO@TiO$_2$** after same exposure time. 92% was reached for **GO@TiO$_2$-500**, which improved compared to 73% reached before calcination. An impressive 99% removal was observed for **PGO@TiO$_2$-500**. The reason for their improved photocatalytic activity could be associated with the thermal treatment that (i) allows for the crystallization of the amorphous species to generate the more active semiconducting phase and (ii) reduce the oxygenated groups on the graphene surface, making the resulting surface more conductive and much more efficient to delay hole–electron recombination during photo-oxidation.

The recycling of the photocatalyst was also assessed, which demonstrated that the grown anatase–rutile could be removed and reused several times (Fig. S2†). However, a substantial deactivation is also observed, which further necessitated the optimization of the recycling conditions. The blank experiments using graphene derivatives have revealed the interesting adsorptive ability of these materials toward methylene blue, in agreement with the literature.[67,68] It seems indeed that the performance reached in our materials emanates from the holistic combination of their adsorption ability due the open porous network associated with the photocatalytic activity of the anchored titanium dioxide.

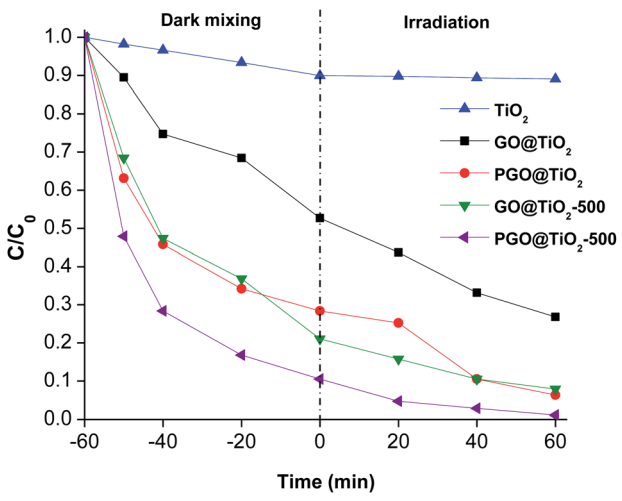

Fig. 7 Adsorption and photocatalytic degradation performance of all the studied materials. Conditions: 50 mg of the photocatalyst, 10^{-4} mmol L^{-1} of methylene blue solution (80 mL). The photocatalyst is suspended under dark conditions for 1 h prior to irradiation.

Experimental section

General

DRUV spectra were measured in the 200–800 nm range using spectral on as the reference on a PerkinElmer Lambda 1050 spectrometer equipped with an integrating sphere (Lapshere, North Sutton, USA). Nitrogen sorption isotherms at 77 K were obtained with a Micromeritics ASAP 2010 apparatus (Micromeritics, Norcross, GA, USA). Prior to measurement, the samples were degassed for 8 h at 80 °C to remove any physisorbed species. The surface area of the samples was evaluated as $S_g = N_m Ar$, where N_m are the N_2 molecules adsorbed in a statistical monolayer on a gram of sample, A is the Avogadro number, and r is the molecular area of adsorbed N_2 (r commonly used being 0.162 nm^2). The values are taken in the range of $0.03 < p/p_0 < 0.3$. X-ray powder diffraction (XRD) patterns were recorded on a D8 Advance Bruker AXS system (Bruker D8 Advance; Bruker Corp, Billerica, MA, EUA) using CuKα radiation with a step size of 0.02° in the 2θ range from 0.45 to 87°. Field Emission Scanning Electron Microscopy (FESEM) images were acquired using a ZEISS ULTRA 55 microscope equipped with an X-ray detector (EDS). Scanning Transmission Electron Microscopy (STEM) images were acquired using a JEOL JEM 2100F Field Emission Transmission Electron Microscope of 200 kV equipped with an X-ray detector. Raman spectra were recorded using a 514 nm excitation laser on a Horiba LabRAM HR Evolution spectrometer.

Synthesis of GO@TiO$_2$ and PGO@TiO$_2$

GO@TiO$_2$ and **PGO@TiO$_2$** were synthesized through a one-pot procedure. 200 mg of **GO** was dispersed in 50 mL of ethanol and sonicated for 90 min. 1.8 mL of Ti(OiPr)$_4$ was added to the suspension and the mixture was stirred at 60 °C for 24 h. The mixture was centrifuged and the collected solid was dispersed in a mixture of H_2O : toluene (10 : 90% (v/v)) and the suspension was allowed to react at 90 °C for 6 h. At the end of the reaction, the product was filtered and thoroughly washed with water and ethanol. **PGO@TiO$_2$** was synthesized following the same procedure used to obtain **GO@TiO$_2$**, using **PGO** instead of **GO**.

Synthesis of GO@TiO$_2$-500 and PGO@TiO$_2$-500

GO@TiO$_2$ or **PGO@TiO$_2$** were thermally annealed at 500 °C for 1 h under N_2 atmosphere using a heating ramp of 5°C min^{-1}.

Photodegradation studies

The photodegradation experiments were carried out by loading 80 mL of methylene blue solutions ($C_0 = 10^{-4}$ mmol L^{-1}) and

50 mg of the photocatalyst. The mixture was kept under constant magnetic stirring in the dark for an hour so that the methylene blue adsorption equilibrium on the catalyst surface was established. Then, we exposed the reaction mixture to radiation. Experiments were performed at room temperature. The samples taken were filtered with Millipore filters having pore sizes equal to 0.45 μm. The remaining concentration of methylene blue in the solution (C) was measured using a previously calibrated UV-vis spectrophotometer. The wavelength of maximum absorption (λ_{max}) is 660 nm. Between each catalytic run, the powder was centrifuged, washed with pure water, and dried at 60 °C for 12 h before the next run.

Conclusion

The association of titanium dioxide and carbon-based nanostructures has been claimed as a promising route toward efficient visible-light activated photo-oxidation catalysts. However, the field has been overwhelmingly dominated by comparing graphene and its forebearers, fullerene and carbon nanotubes, rather than exploring new paths for designing interfacially-tunable graphene-based photocatalysts. Herein, we report a comparative study using **GO@TiO$_2$** and **PGO@TiO$_2$** analogues. We have elucidated the role of surface chemistry for metal oxide growth and crystallization during the post-grafting step. The evolution of the metal oxide and the graphene phase was also assessed during both thermal annealing treatment and upon irradiation. Lastly, we made a comparison based on their performance in the removal of methylene blue pollutant from water. The contrasting activity of graphene-based nanocomposites compared to graphene-free degussa photo-catalyst that is devoid of significant activity highlights the benefits imparted by the presence of graphene support in these materials. Within our series, **PGO@TiO$_2$-500** displayed the highest photo-oxidation activity owing to the holistic combination of improved crystallinity of the metal oxide semiconductor and the surface reduction of the graphitic phase. It can be indeed concluded that both surface phosphorylation and thermal treatment improve the material performance. However, the door is still open for further optimization. We particularly stress that the ratio graphene : titanium dioxide must be varied by increasing the amount of titanium dioxide to determine the optimal contribution of adsorption *versus* photo-oxidation. Residual surface groups must be passivated to prevent poisoning during photocatalysis, with the aim of extending the life-time of the corresponding materials. The next step will focus on wrapping these nanocomposites in polymer-based membranes to assess their practical use in water-cleaning technologies. To sum up, another channel of possibilities could be opened through surface chemistry for the rational design of photoactive graphene-based nanocomposites that could be implemented in water-cleaning technologies.

Conflicts of interest

There are no conflicts to declare.

Acknowledgements

UEMF is acknowledged for the financial support. Authors thank Youssef Ammari for his technical assistance during the preliminary step of the project.

Notes and references

1 C. R. Holkar, A. J. Jadhav, D. V. Pinjari, N. M. Mahamuni and A. B. Pandit, A critical review on textile wastewater treatments: Possible approaches, *J. Environ. Manage.*, 2016, **182**, 351–366.
2 I. Ali, New Generation Adsorbents for Water Treatment, *Chem. Rev.*, 2012, **112**, 5073–5091.
3 D. Cambié, C. Bottecchia, N. J. W. Straathof, V. Hessel and T. Noël, Applications of Continuous-Flow Photochemistry in Organic Synthesis, Material Science, and Water Treatment, *Chem. Rev.*, 2016, **116**, 10276–10341.
4 X. Zhang, A. J. Du, J. Pan, Y. Wang and D. D. Sun, in *New Membranes and Advanced Materials for Wastewater Treatment*, American Chemical Society, 2009, ch. 14, vol. 1022, pp. 219–237.
5 H. Zhang, Y. Zhu, J. Long, Z. Ding, R. Yuan, Z. Li and C. Xu, In situ construction of layered graphene-based nanofiltration membranes with interlayer photocatalytic purification function and their application for water treatment, *Environ. Sci.: Nano*, 2019, **6**, 2195–2202.
6 N. Hilal and C. J. Wright, Exploring the current state of play for cost-effective water treatment by membranes, *npj Clean Water*, 2018, **1**, 8.
7 S. A. Al-Hammadi, A. A. Al-Absi, O. A. Bin-Dahman and T. A. Saleh, Poly(trimesoyl chloride-melamine) grafted on palygorskite for simultaneous ultra-trace removal of methylene blue and toxic metals, *J. Environ. Manage.*, 2018, **226**, 358–364.
8 H. A. Sani, M. B. Ahmad and T. A. Saleh, Synthesis of zinc oxide/talc nanocomposite for enhanced lead adsorption from aqueous solutions, *RSC Adv.*, 2016, **6**, 108819–108827.
9 V. K. Gupta, I. Ali, T. A. Saleh, A. Nayak and S. Agarwal, Chemical treatment technologies for waste-water recycling—an overview, *RSC Adv.*, 2012, **2**, 6380–6388.
10 A. M. Alansi, W. Z. Alkayali, M. H. Al-qunaibit, T. F. Qahtan and T. A. Saleh, Synthesis of exfoliated polystyrene/anionic clay MgAl-layered double hydroxide: structural and thermal properties, *RSC Adv.*, 2015, **5**, 71441–71448.
11 F. Alakhras, E. Alhajri, R. Haounati, H. Ouachtak, A. A. Addi and T. A. Saleh, A comparative study of photocatalytic degradation of rhodamine B using natural-based zeolite composites, *Surf. Interfaces*, 2020, **20**, 100611.
12 A. Fujishima, T. N. Rao and D. A. Tryk, Titanium dioxide photocatalysis, *J. Photochem. Photobiol., C*, 2000, **1**, 1–21.
13 X. Chen and S. S. Mao, Titanium Dioxide Nanomaterials: Synthesis, Properties, Modifications, and Applications, *Chem. Rev.*, 2007, **107**, 2891–2959.
14 J. Schneider, M. Matsuoka, M. Takeuchi, J. Zhang, Y. Horiuchi, M. Anpo and D. W. Bahnemann,

Understanding TiO_2 Photocatalysis: Mechanisms and Materials, *Chem. Rev.*, 2014, **114**, 9919–9986.

15 V. Etacheri, C. Di Valentin, J. Schneider, D. Bahnemann and S. C. Pillai, Visible-light activation of TiO_2 photocatalysts: advances in theory and experiments, *J. Photochem. Photobiol., C*, 2015, **25**, 1–29.

16 H. Tong, S. Ouyang, Y. Bi, N. Umezawa, M. Oshikiri and J. Ye, Nano-photocatalytic Materials: Possibilities and Challenges, *Adv. Mater.*, 2012, **24**, 229–251.

17 V. Subramanian, E. Wolf and P. V. Kamat, Semiconductor–Metal Composite Nanostructures. To What Extent Do Metal Nanoparticles Improve the Photocatalytic Activity of TiO_2 Films?, *J. Phys. Chem. B*, 2001, **105**, 11439–11446.

18 P. D. Cozzoli, E. Fanizza, R. Comparelli, M. L. Curri, A. Agostiano and D. Laub, Role of Metal Nanoparticles in TiO_2/Ag Nanocomposite-Based Microheterogeneous Photocatalysis, *J. Phys. Chem. B*, 2004, **108**, 9623–9630.

19 W. Dong, L. Li, X. Chen, Y. Yao, Y. Ru, Y. Sun, W. Hua, G. Zhuang, D. Zhao, S. Yan and W. Song, Mesoporous anatase crystal-silica nanocomposites with large intrawall mesopores presenting quite excellent photocatalytic performances, *Appl. Catal., B*, 2019, **246**, 284–295.

20 M. Besançon, L. Michelin, L. Josien, L. Vidal, K. Assaker, M. Bonne, B. Lebeau and J.-L. Blin, Influence of the porous texture of SBA-15 mesoporous silica on the anatase formation in TiO_2–SiO_2 nanocomposites, *New J. Chem.*, 2016, **40**, 4386–4397.

21 B. J. Aronson, C. F. Blanford and A. Stein, Solution-Phase Grafting of Titanium Dioxide onto the Pore Surface of Mesoporous Silicates: Synthesis and Structural Characterization, *Chem. Mater.*, 1997, **9**, 2842–2851.

22 H. Safardoust-Hojaghan and M. Salavati-Niasari, Degradation of methylene blue as a pollutant with N-doped graphene quantum dot/titanium dioxide nanocomposite, *J. Cleaner Prod.*, 2017, **148**, 31–36.

23 Y. Deng, M. Chen, G. Chen, W. Zou, Y. Zhao, H. Zhang and Q. Zhao, Visible–Ultraviolet Upconversion Carbon Quantum Dots for Enhancement of the Photocatalytic Activity of Titanium Dioxide, *ACS Omega*, 2021, **6**, 4247–4254.

24 Y. Brahmi, N. Katir, A. Hameau, A. Essoumhi, E. M. Essassi, A.-M. Caminade, M. Bousmina, J.-P. Majoral and A. El Kadib, Hierarchically porous nanostructures through phosphonate–metal alkoxide condensation and growth using functionalized dendrimeric building blocks, *Chem. Commun.*, 2011, **47**, 8626–8628.

25 Y. Brahmi, N. Katir, M. Ianchuk, V. Collière, E. M. Essassi, A. Ouali, A.-M. Caminade, M. Bousmina, J. P. Majoral and A. El Kadib, Low temperature synthesis of ordered mesoporous stable anatase nanocrystals: the phosphorus dendrimer approach, *Nanoscale*, 2013, **5**, 2850–2856.

26 Y. Brahmi, N. Katir, J. A. M. Agullo, A. Primo, M. Bousmina, J. Pierre Majoral, H. Garcia and A. El Kadib, Organophosphonate bridged anatase mesocrystals: low temperature crystallization, thermal growth and hydrogen photo-evolution, *Dalton Trans.*, 2015, **44**, 15544–15556.

27 N. Katir, Y. Brahmi, J. P. Majoral, M. Bousmina and A. El Kadib, Ternary cooperative assembly—polymeric condensation of photoactive viologen, phosphonate-terminated dendrimers and crystalline anatase nanoparticles, *Chem. Commun.*, 2015, **51**, 17716–17719.

28 N. Katir, N. Marcotte, S. Michlewska, M. Ionov, N. El Brahmi, M. Bousmina, J. P. Majoral, M. Bryszewska and A. El Kadib, Dendrimer for Templating the Growth of Porous Catechol-Coordinated Titanium Dioxide Frameworks: Toward Hemocompatible Nanomaterials, *ACS Appl. Nano Mater.*, 2019, **2**, 2979–2990.

29 K. Woan, G. Pyrgiotakis and W. Sigmund, Photocatalytic Carbon-Nanotube–TiO_2 Composites, *Adv. Mater.*, 2009, **21**, 2233–2239.

30 D. Eder and A. H. Windle, Carbon–Inorganic Hybrid Materials: The Carbon-Nanotube/TiO_2 Interface, *Adv. Mater.*, 2008, **20**, 1787–1793.

31 A. Jitianu, T. Cacciaguerra, R. Benoit, S. Delpeux, F. Béguin and S. Bonnamy, Synthesis and characterization of carbon nanotubes–TiO_2 nanocomposites, *Carbon*, 2004, **42**, 1147–1151.

32 Y. Yao, G. Li, S. Ciston, R. M. Lueptow and K. A. Gray, Photoreactive TiO_2/Carbon Nanotube Composites: Synthesis and Reactivity, *Environ. Sci. Technol.*, 2008, **42**, 4952–4957.

33 A. K. Geim and K. S. Novoselov, The rise of graphene, *Nat. Mater.*, 2007, **6**, 183–191.

34 S. Stankovich, D. A. Dikin, G. H. B. Dommett, K. M. Kohlhaas, E. J. Zimney, E. A. Stach, R. D. Piner, S. T. Nguyen and R. S. Ruoff, Graphene-based composite materials, *Nature*, 2006, **442**, 282–286.

35 H. Chang and H. Wu, Graphene-based nanocomposites: preparation, functionalization, and energy and environmental applications, *Energy Environ. Sci.*, 2013, **6**, 3483–3507.

36 K. S. Novoselov, A. K. Geim, S. V. Morozov, D. Jiang, Y. Zhang, S. V. Dubonos, I. V. Grigorieva and A. A. Firsov, Electric Field Effect in Atomically Thin Carbon Films, *Science*, 2004, **306**, 666–669.

37 N. Zhang, M.-Q. Yang, S. Liu, Y. Sun and Y.-J. Xu, Waltzing with the Versatile Platform of Graphene to Synthesize Composite Photocatalysts, *Chem. Rev.*, 2015, **115**, 10307–10377.

38 Y. Liu, D. Zhang, Y. Shang, W. Zang and M. Li, Construction of multifunctional films based on graphene–TiO2 composite materials for strain sensing and photodegradation, *RSC Adv.*, 2015, **5**, 104785–104791.

39 Z. Qianqian, B. Tang and H. Guoxin, High photoactive and visible-light responsive graphene/titanate nanotubes photocatalysts: Preparation and characterization, *J. Hazard. Mater.*, 2011, **198**, 78–86.

40 W. Li, F. Wang, S. Feng, J. Wang, Z. Sun, B. Li, Y. Li, J. Yang, A. A. Elzatahry, Y. Xia and D. Zhao, Sol–Gel Design Strategy for Ultradispersed TiO_2 Nanoparticles on Graphene for High-Performance Lithium Ion Batteries, *J. Am. Chem. Soc.*, 2013, **135**, 18300–18303.

41 M. S. A. Sher Shah, A. R. Park, K. Zhang, J. H. Park and P. J. Yoo, Green Synthesis of Biphasic TiO_2–Reduced Graphene Oxide Nanocomposites with Highly Enhanced

Photocatalytic Activity, *ACS Appl. Mater. Interfaces*, 2012, **4**, 3893–3901.

42 W. R. Gallegos-Pérez, A. C. Reynosa-Martínez, C. Soto-Ortiz, M. Angélica Álvarez-Lemus, J. Barroso-Flores, V. García Montalvo and E. López-Honorato, Effect of UV radiation on the structure of graphene oxide in water and its impact on cytotoxicity and As(III) adsorption, *Chemosphere*, 2020, **249**, 126160.

43 J. G. Radich, A. L. Krenselewski, J. Zhu and P. V. Kamat, Is Graphene a Stable Platform for Photocatalysis? Mineralization of Reduced Graphene Oxide With UV-Irradiated TiO_2 Nanoparticles, *Chem. Mater.*, 2014, **26**, 4662–4668.

44 Y. Zhang, Z.-R. Tang, X. Fu and Y.-J. Xu, TiO_2–Graphene Nanocomposites for Gas-Phase Photocatalytic Degradation of Volatile Aromatic Pollutant: Is TiO_2–Graphene Truly Different from Other TiO_2–Carbon Composite Materials?, *ACS Nano*, 2010, **4**, 7303–7314.

45 Y. Zhang, Z.-R. Tang, X. Fu and Y.-J. Xu, Engineering the Unique 2D Mat of Graphene to Achieve Graphene–TiO_2 Nanocomposite for Photocatalytic Selective Transformation: What Advantage does Graphene Have over Its Forebear Carbon Nanotube?, *ACS Nano*, 2011, **5**, 7426–7435.

46 A. Anouar, N. Katir, A.-S. Mamede, A. Aboulaich, K. Draoui, S. Royer and A. El Kadib, Synthesis and multifaceted use of phosphorylated graphene oxide: growth of titanium dioxide clusters, interplay with gold nanoparticles and exfoliated sheets in bioplastics, *Mater. Chem. Front.*, 2019, **3**, 242–250.

47 N. Wrońska, A. Anouar, M. El Achaby, K. Zawadzka, M. Kędzierska, K. Miłowska, N. Katir, K. Draoui, S. Różalska, I. Piwoński, M. Bryszewska, A. El Kadib and K. Lisowska, Chitosan-Functionalized Graphene Nanocomposite Films: Interfacial Interplay and Biological Activity, *Materials*, 2020, **13**, 998.

48 W. S. Hummers and R. E. Offeman, Preparation of Graphitic Oxide, *J. Am. Chem. Soc.*, 1958, **80**, 1339.

49 J. I. Paredes, S. Villar-Rodil, A. Martínez-Alonso and J. M. D. Tascón, Graphene Oxide Dispersions in Organic Solvents, *Langmuir*, 2008, **24**, 10560–10564.

50 P. Serp and B. Machado, *Nanostructured Carbon Materials for Catalysis*, The Royal Society of Chemistry, 2015, pp. 1–45.

51 M. C. Román-Martínez, D. Cazorla-Amorós, A. Linares-Solano, C. S.-M. n. De Lecea, H. Yamashita and M. Anpo, Metal-support interaction in Pt/C catalysts. Influence of the support surface chemistry and the metal precursor, *Carbon*, 1995, **33**, 3–13.

52 W. Ma, Z. Lu and M. Zhang, Investigation of structural transformations in nanophase titanium dioxide by Raman spectroscopy, *Appl. Phys. A*, 1998, **66**, 621–627.

53 G. Guerrero, J. G. Alauzun, M. Granier, D. Laurencin and P. H. Mutin, Phosphonate coupling molecules for the control of surface/interface properties and the synthesis of nanomaterials, *Dalton Trans.*, 2013, **42**, 12569–12585.

54 G. Guerrero, P. H. Mutin and A. Vioux, Anchoring of Phosphonate and Phosphinate Coupling Molecules on Titania Particles, *Chem. Mater.*, 2001, **13**, 4367–4373.

55 P. H. Mutin, G. Guerrero and A. Vioux, Hybrid materials from organophosphorus coupling molecules, *J. Mater. Chem.*, 2005, **15**, 3761–3768.

56 S. El Hankari, N. Katir, V. Collière, Y. Coppel, M. Bousmina, J. P. Majoral and A. El Kadib, Urea-assisted cooperative assembly of phosphorus dendrimer–zinc oxide hybrid nanostructures, *New J. Chem.*, 2019, **43**, 2141–2147.

57 K. Milowska, A. Rybczyńska, J. Mosiolek, J. Durdyn, E. M. Szewczyk, N. Katir, Y. Brahmi, J.-P. Majoral, M. Bousmina, M. Bryszewska and A. El Kadib, Biological Activity of Mesoporous Dendrimer-Coated Titanium Dioxide: Insight on the Role of the Surface–Interface Composition and the Framework Crystallinity, *ACS Appl. Mater. Interfaces*, 2015, **7**, 19994–20003.

58 M. A. Pizzoccaro-Zilamy, S. M. Piña, B. Rebiere, C. Daniel, D. Farrusseng, M. Drobek, G. Silly, A. Julbe and G. Guerrero, Controlled grafting of dialkylphosphonate-based ionic liquids on γ-alumina: design of hybrid materials with high potential for CO_2 separation applications, *RSC Adv.*, 2019, **9**, 19882–19894.

59 L. S. K. Achary, A. Kumar, L. Rout, S. V. S. Kunapuli, R. S. Dhaka and P. Dash, Phosphate functionalized graphene oxide with enhanced catalytic activity for Biginelli type reaction under microwave condition, *Chem. Eng. J.*, 2018, **331**, 300–310.

60 A. M. Alansi, T. F. Qahtan and T. A. Saleh, Solar-Driven Fixation of Bismuth Oxyhalides on Reduced Graphene Oxide for Efficient Sunlight-Responsive Immobilized Photocatalytic Systems, *Adv. Mater. Interfaces*, 2021, **8**, 2001463.

61 L. Zhang, S. Diao, Y. Nie, K. Yan, N. Liu, B. Dai, Q. Xie, A. Reina, J. Kong and Z. Liu, Photocatalytic Patterning and Modification of Graphene, *J. Am. Chem. Soc.*, 2011, **133**, 2706–2713.

62 G. Williams, B. Seger and P. V. Kamat, TiO_2-Graphene Nanocomposites. UV-Assisted Photocatalytic Reduction of Graphene Oxide, *ACS Nano*, 2008, **2**, 1487–1491.

63 N. R. Ostyn, B. Thijs, J. A. Steele, S. P. Sree, W. Wangermez, J. Teyssandier, M. M. Minjauw, J. Li, C. Detavernier, M. B. J. Roeffaers, S. De Feyter and J. A. Martens, Controlled graphite surface functionalization using contact and remote photocatalytic oxidation, *Carbon*, 2021, **172**, 637–646.

64 K. Spilarewicz-Stanek, A. Jakimińska, A. Kisielewska, M. Dudek and I. Piwoński, Graphene oxide photochemical transformations induced by UV irradiation during photocatalytic processes, *Mater. Sci. Semicond. Process.*, 2021, **123**, 105525.

65 P. C. Ricci, C. M. Carbonaro, L. Stagi, M. Salis, A. Casu, S. Enzo and F. Delogu, Anatase-to-Rutile Phase Transition in TiO_2 Nanoparticles Irradiated by Visible Light, *J. Phys. Chem. C*, 2013, **117**, 7850–7857.

66 J. Criado and C. Real, Mechanism of the inhibiting effect of phosphate on the anatase → rutile transformation induced

by thermal and mechanical treatment of TiO_2, *J. Chem. Soc., Faraday Trans. 1*, 1983, **79**, 2765–2771.

67 T. Liu, Y. Li, Q. Du, J. Sun, Y. Jiao, G. Yang, Z. Wang, Y. Xia, W. Zhang, K. Wang, H. Zhu and D. Wu, Adsorption of methylene blue from aqueous solution by graphene, *Colloids Surf., B*, 2012, **90**, 197–203.

68 W. Zhang, C. Zhou, W. Zhou, A. Lei, Q. Zhang, Q. Wan and B. Zou, Fast and Considerable Adsorption of Methylene Blue Dye onto Graphene Oxide, *Bull. Environ. Contam. Toxicol.*, 2011, **87**, 86.